Energy Increase in Multi-MeV Ion Acceleration in the Interaction of a Short Pulse Laser with a Cluster-Gas Target

Y. Fukuda,[1] A. Ya. Faenov,[1] M. Tampo,[1] T. A. Pikuz,[1] T. Nakamura,[1] M. Kando,[1] Y. Hayashi,[1] A. Yogo,[1] H. Sakaki,[1] T. Kameshima,[1] A. S. Pirozhkov,[1] K. Ogura,[1] M. Mori,[1] T. Zh. Esirkepov,[1] J. Koga,[1] A. S. Boldarev,[2] V. A. Gasilov,[2] A. I. Magunov,[3] T. Yamauchi,[4] R. Kodama,[5] P. R. Bolton,[1] Y. Kato,[1] T. Tajima,[1] H. Daido,[1] and S. V. Bulanov[1,3]

[1]*Kansai Photon Science Institute and Photo-Medical Research Center, JAEA, Kyoto, 615-0215 Japan*
[2]*Institute of Mathematical Modeling, Russian Academy of Sciences, Moscow, 125047 Russia*
[3]*A. M. Prokhorov Institute of General Physics, Russian Academy of Sciences, Moscow, 119991 Russia*
[4]*Graduate School of Maritime Sciences, Kobe University, Kobe 658-0022, Japan*
[5]*Faculty of Engineering and Institute of Laser Engineering, Osaka University, Osaka, 565-0871 Japan*

(Received 6 April 2009; published 13 October 2009)

An approach for accelerating ions, with the use of a cluster-gas target and an ultrashort pulse laser of 150-mJ energy and 40-fs duration, is presented. Ions with energy 10–20 MeV per nucleon having a small divergence (full angle) of 3.4° are generated in the forward direction, corresponding to approximately tenfold increase in the ion energies compared to previous experiments using solid targets. It is inferred from a particle-in-cell simulation that the high energy ions are generated at the rear side of the target due to the formation of a strong dipole vortex structure in subcritical density plasmas.

DOI: 10.1103/PhysRevLett.103.165002 PACS numbers: 52.38.Kd, 52.38.Hb, 52.65.Rr

The recent development of ultrashort-pulse high peak power laser systems enables us to investigate high field science under extreme conditions [1]. Ion acceleration has been one of the most active areas of research in high field science during the last several years [2], due to the broad range of applications in cancer therapy [3,4], isotope preparation for medical applications [5], proton radiography [6], and controlled thermonuclear fusion [7].

Multi-MeV ions have been generated in overdense plasmas with thin foil targets [8], where the proton acceleration has been interpreted as target normal sheath acceleration (TNSA) [9] (see for details Refs. [10]). Generation of multi-MeV ions has been also demonstrated in underdense plasmas, produced either by direct ionization of gas targets [11,12] or by evaporation of thin solid targets by the laser prepulse [13]. Ions are accelerated radially in Refs. [11] by a collisionless shock acceleration mechanism, while in the case of Refs. [12,13], an electric field is generated at the plasma-vacuum interface through a combination of charge separation and a quasistatic magnetic field produced by the fast electron current which can accelerate ions in the forward direction and collimate them radially [14]. The effect of the quasistatic magnetic field is dominant for the shorter laser pulse lengths in Refs. [13]. Quasimonoenergetic ions can be generated using microstructured targets [4,15]. The divergence and the energy spread of ions can be controlled with a plasma microlens [16] or magnet systems [17]. Recent improvement of the contrast ratio of laser pulses allowed the ion energy increase by decreasing the target thickness [18]. These advances establish a firm basis for realizing various applications of laser-driven ions. One of the important aims is the enhancement of the ion energy to the range usable in cancer therapy [3,4].

Here we describe the high energy ion generation in a cluster-gas target irradiated by an ultrashort pulse laser. Cluster targets have shown unique properties such as formation of an efficient plasma waveguide [19] and generation of copious high energy electrons [20]. These are advantageous for effective acceleration of ions, because the plasma waveguide facilitates the intense laser pulse transport over a long distance and a large number of fast electrons creates strong electric fields. Furthermore, the replenishable cluster target enables high repetition rate of high energy ion generation, free of plasma debris. We note that our approach is different from ion acceleration due to the Columb explosion of clusters [21]. Our target is a cloud of solid-density submicron-size clusters embedded in a background gas. Under the action of the prepulse accompanying the main laser pulse, the clusters are expected to be evaporated forming a subcritical inhomogeneous plasma with its profile determined by the initial density distribution of the cluster-gas target.

The experiment has been conducted using the JLITE-X 4-TW Ti:sapphire laser at JAEA-KPSI. A schematic of the experimental setup is shown in Fig. 1(a). The laser delivers 40-fs duration (FWHM) pulses of 150 mJ energy at a 1 Hz repetition rate with a contrast ratio of 10^{-6}. A pulsed solenoid valve connected to a specially designed circular nozzle having a three-stage conical structure with an orifice diameter of 2 mm was used to produce submicron-size CO_2 clusters embedded in He gas. With the aid of a numerical model [22], we find that a 60-bar gas consisting of 90% He and 10% CO_2 is optimal for the production of submicron-size CO_2 clusters. The reliability of the model has been verified by an experiment with the use of Rayleigh scattering of the light from the clusters [23]. The laser pulse was split into a main pulse and a lower

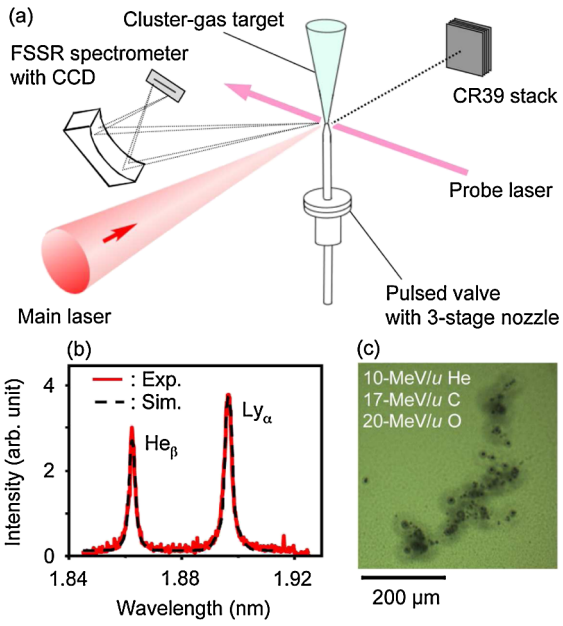

FIG. 1 (color online). (a) Schematic of the experimental setup. (b) Measured (solid curve) and calculated (dotted curve) soft x-ray spectra for the subcritical density plasma of the order of 10^{20} cm^{-3} which is about $0.1n_c$. (c) Typical images of the etched pits registered in the 11th layer of CR39.

energy probe pulse. The main laser pulse was focused to a 30-μm diameter spot ($1/e^2$ intensity) with an off-axis parabola having an effective focal length of 646 mm. This yields a peak vacuum intensity of 7×10^{17} W/cm^2. The high energy ions were generated when the laser beam was focused near the rear side of the gas jet, 1.5 mm above the nozzle orifice, Fig. 2(a). Using the model described in Ref. [22], we calculated that at this position, solid-density CO_2 clusters with an average diameter of 0.4 μm (a root mean square deviation of 0.1 μm), containing 5×10^8 molecules each, are embedded in the He gas of density 2×10^{19} cm^{-3} which corresponds to $\sim 0.02n_c$, where $n_c = m_e\omega^2/4\pi e^2$ is the critical density. Here a high cluster density (3×10^9 cm^{-3}) and a small intercluster distance (5 μm) are achieved. It is expected that significant enhancement of the laser intensity occurs during its propagation through the target, because the peak power of the main laser pulse is well above the critical power for relativistic self-focusing. The laser propagation in the target was monitored by shadowgraph images with the probe laser. The shadowgraph image shown in Fig. 2(a) reveals the formation of a channel of approximately 5 mm in length, substantially longer than the nozzle orifice diameter (2 mm) and the Rayleigh length (900 μm). The plasma condition was monitored by measuring soft x-ray spectra of the He$_\beta$ (665.7 eV) and Ly$_\alpha$ (653.7 eV) lines of oxygen using a focusing spectrometer with spatial resolution (FSSR) [24] equipped with a spherically bent mica crystal and a back illuminated CCD camera, Fig. 1(b).

The high energy ions were measured with a stack of solid state nuclear track detectors (SSNTD) placed on the

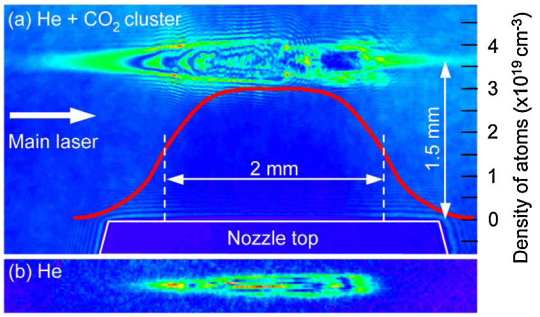

FIG. 2 (color online). (a) The shadowgraph image for a mixture of He gas and CO_2 clusters. The red (or gray) line shows the initial atom density profile. (b) The shadowgraph image for a pure He gas target.

laser propagation axis at a distance 200 mm from the laser focal plane. The SSNTD stack consisted of ten sheets of 10-μm thick polycarbonate film and 12 sheets of 100-μm thick CR39 with an area of 40×40 mm^2. A single 6-μm Al foil was placed in front of this track detector to protect it from damage induced by the transmitted portion of the main laser pulse. Ions were accumulated for about six thousand laser shots. Figure 1(c) shows a typical image of the etched pits, which was registered in the 11th layer of the CR39, observed with a differential interference microscope. Observations of the pit images through the whole layers of CR39 reveal that these pits penetrate through several successive CR39 layers at exactly the same lateral and vertical positions, and vanish at some layers which correspond to the depth of the Bragg peak for ions in the CR39 stack. The track images also show that these high energy ions are well collimated with a divergence (full angle) of 3.4° in the forward direction.

The energy range of the ions is determined quantitatively from the extent of the tracks recorded in the CR-39 stack by calculating their stopping ranges. Since the target is a mixture of He gas and CO_2 clusters, highly charged ions of helium, carbon, and oxygen are the possible candidates for accelerated ions. We observe the ion tracks in CR39 up to the 11th layer and none in the 12th layer. This penetration depth corresponds to maximum energies of 10, 17, and 20 MeV per nucleon for helium, carbon, and oxygen ions, respectively. We note that the diameter of the etched pits has two-humped distribution. Since the track registration sensitivity depends strongly on the ion charge [25], we ascribe that the smaller ones are due to the helium ions and the larger ones to the carbon and/or oxygen ions.

Further evidence for high energy ion production was obtained from the time-of-flight (TOF) measurements using a microchannel plate (MCP) detector placed 930-mm downstream from the gas nozzle along the laser propagation axis in place of the SSNTD stack. An electromagnet of field magnitude ~ 0.15 T was placed between the laser focal plane and the MCP to deflect accelerated electrons with energies below 20 MeV. Three layers of the 13-μm thick Al foils were inserted in front of the MCP to block the

transmitted portion of the main laser pulse and to reduce the incident x rays. Helium, carbon, and oxygen ions with the energies exceeding 1.9, 3.2, and 3.6 MeV per nucleon, respectively, could reach the MCP. As shown in the inset in Fig. 3, the MCP registers a real time ion signal from each repetitive laser shot. Figure 3 shows an ion energy spectrum thus obtained from the TOF measurements over 285 consecutive laser shots. The energy scale of the abscissa was calculated assuming the observed ion signals to be those of carbon. The maximum ion energy is measured to be 18.5 ± 1 MeV per nucleon, which is consistent with the energy observed with the CR-39 track detectors.

When a larger prepulse with the contrast ratio of 10^{-4} was intentionally introduced to destroy the clusters well before the arrival of the main pulse, neither a long channel nor ion acceleration was observed. Furthermore, when the laser was focused onto a 60-bar He gas jet of density $\simeq 0.02 n_c$ without clusters using the same nozzle, the rear part of the channel structure as well as the fringe pattern disappeared, Fig. 2(b), and no high energy ions were observed. These results clearly show that the clusters are necessary for retaining the plasma density and its profile in order to make them favorable for the long channel formation and the ion acceleration.

In order to elucidate the ion acceleration process, we conducted two-dimensional particle-in-cell (PIC) simulations, where we assume that the laser intensity is 1×10^{19} W/cm^2 which includes the effect of intensity enhancement due to self-focusing, and the plasma parameters correspond to those of the experiment; i.e., a homogeneous plasma with the maximum density of $0.1 n_c$ is assumed as follows. The plasma is composed of electrons and ions with the atomic number to the nucleon number ratio of $Z/A = 1/2$, i.e., He^{2+}, C^{6+} and O^{8+}, which can be produced via field ionization and/or collisional ionization. As mentioned above, high energy ion generation has been observed when the laser pulse is focused near the rear side of the gas jet. This region of plasma is simulated in the interval $2 < x < 112$ μm. The density is equal to $0.02 n_c$ for $2 < x < 13$ μm, then linearly increases to $0.1 n_c$ for $13 < x < 20$ μm, then remains constant for $20 < x < 65$ μm, then linearly decreases to $0.02 n_c$ for $65 < x < 82$ μm, and then remains constant again for $82 < x < 112$ μm. The plasma slab is surrounded by vacuum regions. The density gradient employed for the PIC simulations is derived from the cluster-gas target model calculation [22]. The rear part of the density profile is shown in Fig. 4(a) with the red (or gray) line.

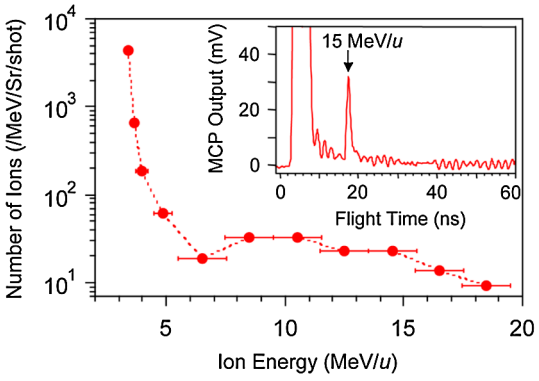

FIG. 3 (color online). The ion energy spectrum obtained by the TOF method. The inset shows TOF spectrum obtained in one laser shot which registers 15 MeV/u ion signal. A saturated signal around the flight time $t = 5$ is caused by hard x rays emitted from the laser-cluster interaction region.

The linearly polarized (y direction) laser pulse propagates along the x axis from the left to the right. The laser pulse forms a channel in the plasma and undergoes relativistic self-focusing, Fig. 4(a). In the region $70 < x < 90$ μm, corresponding to the rear plasma slope, fast electrons accelerated in the channel form a dipole vortex [14], associated with the strong quasistatic bipolar magnetic field with a maximum intensity of about 35 MG as seen in Fig. 4(b). The magnetic field presses out the cold plasma electrons forming the low density regions surrounded by dense thin shells. The density profile in Fig. 4(a) resembles a bilobed structure at the end of the channel seen in the shadowgraph image, Fig. 2(a). The fast electrons produce a quasistatic electric field at the plasma-vacuum interface [Fig. 4(c), region $x > 112$ μm], which is associated with the TNSA acceleration mechanism. However, we find that a much stronger electric field is generated at the shells wrapping the dipole vortex [Fig. 4(c), region $70 < x < 90$ μm].

According to the simulations and Refs. [14], ions are accelerated along the laser propagation axis in a time-dependent electric field generated during the magnetic field annihilation. This process is similar to the ion acceleration in plasma pinch discharges [26]. In the experiment,

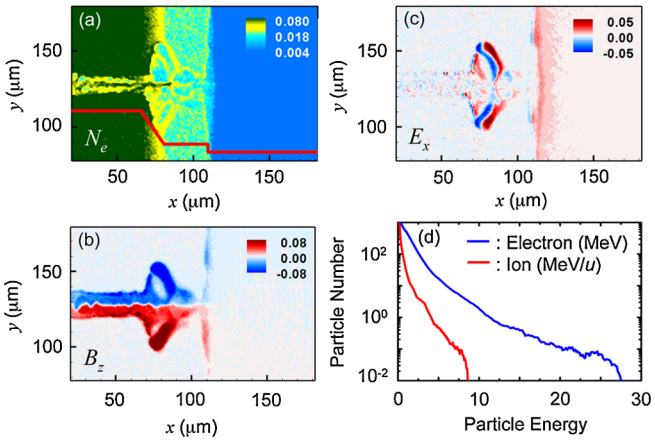

FIG. 4 (color online). The results of 2D PIC simulation. (a) The electron density N_e normalized by n_c. The red (or gray) line shows the initial density profile. (b) The magnetic field B_z normalized by the laser field, and (c) the longitudinal electric field E_x normalized by the laser field at $t = 900$ fs, respectively. (d) The calculated spectra of the ions in units of MeV/u and the electrons in MeV at $t = 6$ ps.

we have observed the ions accelerated in the forward direction. In addition, ions are accelerated perpendicular to the shell surface formed by the inhomogeneous magnetic field pressure. The second component of fast ions is expected to be seen in the direction at about $\pm 45°$ from the laser axis and therefore it could not be observed in the experiment. In the simulations we found that both ion components are well collimated with a divergence (full angle) of 5°. This agrees well with the experimental observation (3.4°). Both components give comparable ion energies with the maximum of 8.5 MeV per nucleon, Fig. 4(d). The electrons have a quasithermal energy spectrum with an effective temperature of 1.9 MeV and a maximum energy of ~20 MeV, Fig. 4(d). Our simulations suggest that the increase of the areal density of the target, nl, and the energy of the laser pulse will result in the increase of the ion energy.

In the presented simulations, the contribution of the TNSA mechanism acting at the plasma-vacuum interface to ion energies is estimated to be about 2 MeV per nucleon. Thus, for our experimental conditions, the formation of the dipole vortex structure is essential for high energy ion generation. Our computer simulations indicate that generation of a favorable magnetic field requires an optimal electron density ($\sim 0.1 n_c$ in our case) and an optimal slope-step profile. In the present experiment, the optimal electron density can not be provided only by the background He gas ($\sim 0.02 n_c$), but can be ensured by a contribution from CO_2 clusters which are initially at solid density and expand during the laser irradiation. In fact, analysis of the soft x-ray spectrum shown in Fig. 1(b) determines the electron density to be $1.0 \pm 0.2 \times 10^{20}$ cm^{-3} which is about $0.1 n_c$. Thus, the use of a mixture of He gas and CO_2 clusters is crucial for securing the proper electron density and the slope-step profile.

In conclusion, we have demonstrated efficient generation of high energy ions with energies up to 10–20 MeV per nucleon and with a small full-angle divergence of 3.4° by irradiating the replenishable cluster-gas target with 40-fs laser pulses of only 150 mJ energy at 1 Hz repetition rate. This corresponds to approximately tenfold improvement of the accelerated ion energy compared to previous experiments with solid targets, where 1.3–1.5 MeV protons were produced using ultrashort laser pulses (<100 fs) with energies of 120–200 mJ [27]. We note that 40 MeV (10 MeV per nucleon) He^{2+} ions were produced using 1-ps laser pulses with a laser energy of 340 J in underdense helium plasma ($\sim 0.04 n_c$) [12]. In our experiment, we have produced subcritical density plasma ($\sim 0.1 n_c$) using a cluster-gas target, which enabled us to accelerate ions up to 10–20 MeV per nucleon, comparable to Refs. [12], using ultrashort laser pulses with ~1000 times lower energy. The demonstrated approach has the potential for constructing compact, high repetition rate laser-driven ion sources for hadron therapy and other applications.

This work was supported by the Special Coordination Funds (SCF) for Promoting Science and Technology commissioned by MEXT of Japan. We are grateful to Professor M. Abe for valuable comments.

[1] G. A. Mourou *et al.*, Rev. Mod. Phys. **78**, 309 (2006).
[2] M. Borghesi *et al.*, Fusion Sci. Technol. **49**, 412 (2006); J. Fuchs *et al.*, Nature Phys. **2**, 48 (2006); L. Robson *et al. ibid.* **3**, 58 (2007).
[3] T. Tajima, J. Jpn. Soc. Therapy. Rad. Oncol. **9**, 83 (1998).
[4] S. V. Bulanov *et al.*, Plasma Phys. Rep. **28**, 453 (2002).
[5] I. Spencer *et al.*, Nucl. Instrum. Methods Phys. Res., Sect. B **183**, 449 (2001).
[6] M. Borghesi *et al.*, Phys. Plasmas **9**, 2214 (2002).
[7] M. Roth *et al.*, Phys. Rev. Lett. **86**, 436 (2001).
[8] E. L. Clark *et al.*, Phys. Rev. Lett. **84**, 670 (2000); A. Maksimchuk *et al.*, *ibid.* **84**, 4108 (2000); R. A. Snavely *et al.*, *ibid.* **85**, 2945 (2000).
[9] S. P. Hatchett *et al.*, Phys. Plasmas **7**, 2076 (2000).
[10] A. V. Gurevich *et al.*, Sov. Phys. JETP **22**, 449 (1966); Y. Kishimoto *et al.*, Phys. Fluids **26**, 2308 (1983); F. Mako *et al. ibid.* **27**, 1815 (1984); P. Mora, Phys. Rev. Lett. **90**, 185002 (2003); M. Passoni *et al.*, *ibid.* **101**, 115001 (2008).
[11] G. S. Sarkisov *et al.*, Phys. Rev. E **59**, 7042 (1999); K. Krushelnick *et al.*, Phys. Rev. Lett. **83**, 737 (1999); M. S. Wei *et al.*, *ibid.* **93**, 155003 (2004).
[12] L. Willingale *et al.*, Phys. Rev. Lett. **96**, 245002 (2006); L. Willingale *et al.*, *ibid.* **98**, 049504 (2007).
[13] K. Matsukado *et al.*, Phys. Rev. Lett. **91**, 215001 (2003); A. Yogo *et al.*, Phys. Rev. E **77**, 016401 (2008).
[14] A. V. Kuznetsov *et al.*, Plasma Phys. Rep. **27**, 211 (2001); S. V. Bulanov *et al.*, *ibid.* **31**, 369 (2005); S. V. Bulanov and T. Zh. Esirkepov, Phys. Rev. Lett. **98**, 049503 (2007).
[15] T. Zh. Esirkepov *et al.*, Phys. Rev. Lett. **89**, 175003 (2002); B. M. Hegelich *et al.*, Nature (London) **439**, 441 (2006); H. Schwoerer *et al.*, *ibid.* **439**, 445 (2006).
[16] T. Toncian *et al.*, Science **312**, 410 (2006).
[17] W. Luo *et al.*, Med. Phys. **32**, 794 (2005); S. Ter-Avetisyan *et al.*, Laser Part. Beams **26**, 637 (2008); M. Schollmeier *et al.*, Phys. Rev. Lett. **101**, 055004 (2008); M. Nishiuchi *et al.*, Appl. Phys. Lett. **94**, 061107 (2009).
[18] T. Ceccotti *et al.*, Phys. Rev. Lett. **99**, 185002 (2007).
[19] I. Alexeev *et al.*, Phys. Rev. Lett. **90**, 103402 (2003).
[20] Y. Fukuda *et al.*, Phys. Lett. A **363**, 130 (2007).
[21] E. Springate *et al.*, Phys. Rev. A **61**, 063201 (2000); M. Eloy *et al.*, Phys. Plasmas **8**, 1084 (2001); K. Nishihara *et al.*, Nucl. Instrum. Methods Phys. Res., Sect. A **464**, 98 (2001).
[22] A. S. Boldarev *et al.*, Rev. Sci. Instrum. **77**, 083112 (2006).
[23] F. Dorchies *et al.*, Phys. Rev. A **68**, 023201 (2003).
[24] A. Ya. Faenov *et al.*, Phys. Scr. **50**, 333 (1994).
[25] B. Dörschel *et al.*, Radiat. Meas. **35**, 287 (2002).
[26] N. V. Filippov, JETP Lett. **31**, 120 (1980).
[27] I. Spencer *et al.*, Phys. Rev. E **67**, 046402 (2003); Y. Oishi *et al.*, Phys. Plasmas **12**, 073102 (2005).